RSC Advances

PAPER

View Article Online
View Journal | View Issue

Cite this: *RSC Adv.*, 2020, **10**, 28075

Study on the interfacial properties of polymers around a nanoparticle

Chao-Yang Li, *[a] Jian-Hua Huang, [b] Hong Li [c] and Meng-Bo Luo [d]

The interfacial properties of polymer chains on spherical nanoparticles are investigated using off-lattice Monte Carlo simulations. Results show that the number of adsorbed monomers increases whereas the number of adsorbed polymers decreases with increasing the polymer–nanoparticle interaction strength. The interfacial layer thickness is independent of the nanoparticle size and chain length. The interfacial monomers exhibit layering behaviors with three distinct layers. The mobility of monomers in the innermost layer is strongly dependent on the polymer–nanoparticle interaction strength. The interfacial monomers always keep moving, and no glassy layer is present around the nanoparticle. Finally, our results show that the motion of nanoparticle can weaken the adsorption of polymers but does not change the conformational property of adsorbed polymers.

Received 19th June 2020
Accepted 20th July 2020

DOI: 10.1039/d0ra05392a

rsc.li/rsc-advances

1. Introduction

Nanoparticles (NPs) in polymer nanocomposites (PNCs) lead to the appearance of new interfaces. PNCs have many novel physical properties in comparison to the bulk phase because of the coupling between polymers and NPs.[1–5] For instance, the existence of nano-sized ZnO in natural rubber can increase the tensile strength and tensile modulus.[6,7] The addition of organic NPs in polymer melts produces an increase in the viscosity and therefore shifts the glass transition temperature.[8–10] The addition of silver NPs in polystyrene (PS)/poly(2-vinyl pyridine) (P2VP) can change the electrical behaviors and optical properties.[11] Moreover, NPs, like dendrimers, can play essential roles in the delivery of DNA or drugs in biological systems.[12–14] In medicine, there is growing attention on the topic to develop new and more efficient tools for NP-mediated drug delivery,[15–17] a practice that is already in use for cancer treatment.[18,19] The application of NPs in PNCs has driven an increased interest in experiments, theories, and computer simulations. Therefore, a detailed understanding of the equilibrium and dynamical properties of polymers near surfaces or interfaces of NP is essential for chemical and biological processes.

The influence of NPs on properties of polymers is interesting from the experimental and simulation investigations.[20–24] However, there is still a lack of consistent conclusion on this specific issue. Small Angle Neutron Scattering (SANS) experiments on poly(dimethylsiloxane) (PDMS) containing trimethylsilyl-treated polysilicate NPs showed a decrease in the dimension of PDMS for $\sigma_n \approx R_{G0}$ and an expansion of PDMS for $\sigma_n < R_{G0}$, where σ_n is the diameter of NPs and R_{G0} is the radius of gyration of the polymer in dilute solution.[20] Similarly, SANS experiment observed a 10–20% increase in the radius of gyration R_G of deuterated polystyrene (d-PS) when $\sigma_n < R_{G0}$,[21] and it was confirmed by small angle X-ray scattering (SAXS) experiments.[3] SAXS found that NPs have no measurable effect on R_G of d-PS when $\sigma_n > R_{G0}$.[3] These results imply that the polymer chain swelling is directly related to the ratio R_{G0}/σ_n. However, R_{G0}/σ_n is not the only or crucial parameter for the change of polymer size. Recent molecular dynamics (MD) simulation studies showed that, for $\sigma_n < R_{G0}$ case, the polymers swell if σ_n is larger than the monomer size while they contract if σ_n is smaller than the monomer size.[17] Monte Carlo (MC) simulation studies pointed out that, even for $\sigma_n < R_{G0}$ case, polymer chains can expand, shrink, or be unaffected by NPs.[22,23] Polymer dimensions are highly dependent on the polymer–NP interaction strength and NP–NP distance.[22,23]

It is also essential to understand the dynamic behaviors of the interfacial polymer, including the adsorption/desorption process, the thermal motion, and the diffusion process. Mohammadreza *et al.* found that MCM-41 NPs in the reversible addition-fragmentation chain transfer polymerization (RAFT) can reduce the diffusivity of polymer chains and consequently slow down the propagation reactions.[25] Using dynamic MC simulations, Hao *et al.* found that the diffusivity of polymers is controlled by NPs.[26] Vacatello found that the attraction of NPs can slow the diffusion of polymers.[27,28] And the diffusivity of polymers can be significantly reduced or even to zero if the attraction between polymer and NP is sufficiently strong.[29–31] Moreover, the polymer dynamics is related to the concentration and distribution of NPs. The normal diffusion of polymers in

[a]Department of Physics, Hangzhou Normal University, Hangzhou 311121, China. E-mail: cyli@hznu.edu.cn
[b]Department of Chemistry, Zhejiang Sci-Tech University, Hangzhou 310018, China
[c]Department of Physics, Wenzhou University, Wenzhou 325035, China
[d]Department of Physics, Zhejiang University, Hangzhou 310027, China

dilute solution can be changed to the sub-diffusion in the media with stationary NPs.[32] Although the diffusivity is slowed down by the attracting NPs, it was further pointed out that the polymer shows a normal diffusion in the system with orderly distributed NPs but a sub-diffusion in the system with randomly distributed NPs.[22,23]

It is generally believed that the change in size and dynamics of polymers are induced by the NP's excluded volume effect and polymer–NP interaction. And the interfacial properties of polymers are important factors to understand the behavior of polymers in PNCs. In this paper, we utilize dynamic MC simulation to unravel the interfacial properties of polymers. The adsorption of polymers, the distribution of monomers, and the mobility of interfacial monomers are investigated. We find that the interfacial region of NP can be separated into three layers based on the distribution of monomers. The mean square displacement of monomers (MSD), the fraction of initial monomers $f(t)$, and the mean probability of monomer movement P_{MM} in different interfacial layers are calculated to describe the dynamic properties of monomers. Our results can provide guidance for understanding the core–shell model and the large gradient of segmental mobility from the experiments.[33,34]

2. Model and simulation method

The simulation system is a cube of size $L \times L \times L$ in the x, y, z directions. Periodical Boundary Conditions (PBC) are considered in all three directions. N_p polymers of chain length n are placed in the system. The number density of monomers, $\rho_0 = 0.85$, corresponding to a dense melt according to the work of Allegra.[35] We adopt the chain length $n = 64$ and $N_p = 106$ for the system size $L = 20$. L is much larger than twice the chain radius of gyration R_{G0}, which can prevent polymers from interacting with themselves through PBC. The NP is modeled as a sphere of diameter σ_n and mobility μ. The NP is fixed in the center of the cube if $\mu = 0$. A lot of novel properties have been observed when $R_{G0} \approx \sigma_n$.[36–38] Here $\sigma_n = 5$ is considered, corresponding to the high molecular weight system ($R_{G0}/\sigma_n = 1.13$) according to the experimental research.[33]

Each polymer is modeled as a linear polymer chain by using a typical bead-spring model developed by Kremer and Grest.[39] All the monomers in the polymer are identical. The mass and diameter of monomer are m and σ, respectively. The interaction between non-bonded monomers is defined as a Lennard–Jones (LJ) potential of the form

$$V(r) = \begin{cases} \varepsilon\left[\left(\frac{\sigma}{r}\right)^{12} - 2\left(\frac{\sigma}{r}\right)^{6}\right] + V_0 & \text{for } r < r_c \\ 0 \quad \text{for } r \geq r_c \end{cases}, \qquad (1)$$

where ε is the depth of the potential, r is the center-to-center distance between two monomers. Here the potential is truncated at a cut-off distance $r_c = 2.5\sigma$ and is then shifted to 0 at r_c by setting $V_0 = -\varepsilon\left[\left(\frac{\sigma}{r_c}\right)^{12} - 2\left(\frac{\sigma}{r_c}\right)^{6}\right]$. We consider $\varepsilon = 0.2$ between two non-bonded monomers. The polymer behaves as a self-avoiding walk (SAW) polymer chain at this weak $\varepsilon = 0.2$.[21,22] For the chemically bonded monomers, finitely extensive nonlinear elastic (FENE) interaction is adopted by the form

$$V_{FENE} = \begin{cases} -\frac{k_F}{2}(r_{max} - r_{eq})^2 \ln\left[1 - \left(\frac{r - r_{eq}}{r_{max} - r_{eq}}\right)^2\right] & \text{for } 2r_{eq} - r_{max} < r < r_{max} \\ \infty \quad \text{otherwise} \end{cases} \qquad (2)$$

with equilibrium bond length $r_{eq} = 0.8\sigma$, maximum bond length $r_{max} = 1.3\sigma$, and elastic coefficient $k_F = 100k_BT/\sigma^2$. In this work, we use $k_BT \equiv 1$ and $\sigma \equiv 1$ as units of energy and length, respectively. Here k_B is the Boltzmann constant, and T is the temperature.

The interaction between polymer and NP is modeled by another expanded LJ potential of the form

$$V_{pn}(r) = \begin{cases} \varepsilon_{pn}\left[\left(\frac{\sigma}{r - s}\right)^{12} - 2\left(\frac{\sigma}{r - s}\right)^{6}\right] + V_0' & \text{for } r < r_c \\ 0 \quad \text{for } r \geq r_c \end{cases}, \qquad (3)$$

where ε_{pn} is the LJ interaction strength between polymer and NP and $s = (\sigma_n - \sigma)/2$.[40] Here r is the center-to-center distance between monomer and NP. The polymer–NP interaction is also taken into account by setting $r_c - s = 2.5\sigma$. At the cut-off distance $r_c = s + 2.5\sigma$, we shift the interaction to $V_{pn}(r = r_c) = 0$ by setting $V_0' = -\varepsilon_{pn}\left[\left(\frac{\sigma}{r_c - s}\right)^{12} - 2\left(\frac{\sigma}{r_c - s}\right)^{6}\right]$.

We adopted the off-lattice dynamic MC algorithm and the metropolis algorithm to simulate the random motion of polymer. Dynamic MC algorithm follows the evolution of one element of the statistical ensemble and simulates the time evolution of the system without dealing with the master equation directly.[41] Thus, dynamical MC algorithm is suited to describe dynamic properties such as monomer mobility. At the beginning of the simulation, N_p polymers of length n are grown monomer by monomer according to the self-avoiding regulation in an amplified simulation system of size $L_a \times L_a \times L_a$ ($L_a = 24\sigma$) because the polymers can be produced efficiently in an extensive system. Then, we randomly select one monomer and move it a small distance with dx, dy, and dz in x, y, and z directions. All dx, dy, and dz are random values within $(-\Delta, \Delta)$. Here a small value $\Delta = 0.1\sigma$ is used. The attempted move will be accepted with a probability $P = \min[1, \exp(-\Delta E/k_BT)]$, where ΔE is the energy shift due to the move. The time unit used in this paper is the MC step (MCS), which is arbitrarily defined and can be rescaled to the real-time unit by experiment or MD simulation. In one MCS every monomer tries to move 100 steps on average. The NP in our simulation can move according to the same role as for monomers. The mobility μ of NP is defined as

the ratio of NP's movement steps to monomer's. We reduce the simulation system size L gradually from the initial $L_a = 24\sigma$ to the desired $L = 20\sigma$ with a small length step $\Delta L = 0.05\sigma$ for every 10^5 MCS. For every intermediate L, the coordinates of monomers and NP are multiplied by a factor $(L - \Delta L)/L$ accordingly. The small reduction step and long equilibrium time enable our system to reach equilibrium at every L. We find that the simulation results do not change if we further increase the equilibrium time or reduce the reduction step. When the system size reaches $L = 20\sigma$, the size of the system remains unchanged. The conformational and dynamic properties reported in this paper are obtained from the high density $\rho = 0.85$ at $L = 20\sigma$.

In the paper, the main variables are the polymer–NP interaction strength ε_{pn}, the polymer–NP distance, and the NP mobility μ. Our simulation results are averaged over 1000 independent runs. The statistical errors of our simulation results are found to be so small and can be negligible.

3. Results and discussions

The NP of $\sigma_n = 5\sigma$ is much heavier than monomer if both NP and monomer have the same mass density, which results in a low mobility of NP. For simplification, we mainly simulate the adsorption, distribution, and mobility of interfacial monomers for stationary NP with $\mu = 0$. At last, we study the effects of NP's mobility on the polymers.

3.1. Adsorption of polymers

Polymer chains can be adsorbed on NP due to the attraction of NP or desorbed from NP because of the thermal motion of monomers. At the critical adsorption point (CAP), the fluctuation of polymer–NP contacts is the largest. The CAP is estimated to be $\varepsilon_{pn}^* = 1.5$ for the polymer adsorbed on spherical NP.[42] We define a polymer–NP contact if the center-to-center distance between NP and monomer is less than $\sigma + \sigma_n/2 = 3.5\sigma$ as in this region the attraction is strong. At $\varepsilon_{pn} > \varepsilon_{pn}^*$, the adsorbed and desorbed polymers can be distinguished from the contact number n_{cp}. We define an adsorbed polymer as $n_{cp} > 0$ and a desorbed polymer as $n_{cp} = 0$. At $\varepsilon_{pn} < \varepsilon_{pn}^*$, $n_{cp} > 0$ only means an accidental contact event between polymer and NP because of the random thermal motion of polymers. Thus, we only consider the adsorption case at $\varepsilon_{pn} > \varepsilon_{pn}^*$ in this paper. Besides n_{cp} for each polymer, we also monitor the following two variables to describe the adsorption of polymers. One is the number of adsorbed polymers N_{p_ad}. The other is the number of total adsorbed monomers n_{cn} that counts the number of monomers adsorbed on the NP. Here n_{cn} is the sum of n_{cp} of adsorbed polymers. The adsorption degree is defined as $D_{ap} = n_{cn}/(nN_{p\_ad})$, *i.e.*, the fraction of the adsorbed monomers in all the adsorbed polymer chains.

Fig. 1 presents the dependences of the mean number of adsorbed polymers $\langle N_{p\_ad}\rangle$ and the mean number of total adsorbed monomers $\langle n_{cn}\rangle$ on the polymer–NP interaction strength ε_{pn}. Here $\langle\ \rangle$ represents an ensemble average over all contact states. We can find that $\langle N_{p\_ad}\rangle$ decreases whereas $\langle n_{cn}\rangle$ increases with the increase in ε_{pn}, which results in an increase

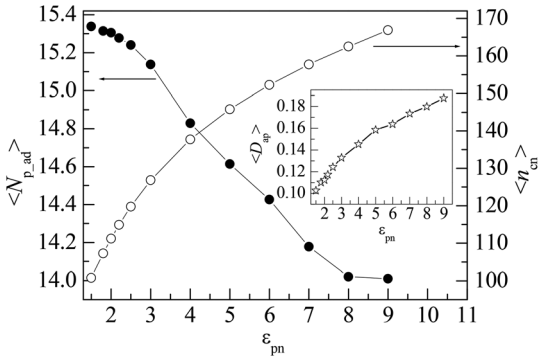

Fig. 1 Dependences of the mean number of adsorbed polymers $\langle N_{p\_ad}\rangle$ and the mean number of total adsorbed monomers $\langle n_{cn}\rangle$ on the polymer–NP interaction strength ε_{pn}, respectively. The inset presents the dependence of the mean adsorption degree of adsorbed polymers $\langle D_{ap}\rangle$ on ε_{pn}. NP mobility $\mu = 0$.

in the mean adsorption degree $\langle D_{ap}\rangle$ with ε_{pn} as shown in the inset of Fig. 1. The variations of $\langle N_{p\_ad}\rangle$ and $\langle n_{cn}\rangle$ with ε_{pn} indicate that the incremental adsorbed monomers mainly come from the already adsorbed polymers and at the same time some of the adsorbed polymers are pushed away because of the excluded volume of the newly adsorbed monomers. The adsorption of the polymer will reduce the conformational entropy. Therefore, the simultaneous adsorption of too many chains is bad for free energy.

The attractive NP may change the polymer conformation which is usually characterized by the mean square radius of gyration $\langle R_G^2\rangle$. We calculate $\langle R_G^2\rangle$ of all adsorbed polymers. Fig. 2 presents the dependence of $\langle R_G^2\rangle$ on the number of polymer–NP contacts n_{cp} for several ε_{pn}s. $\langle R_G^2\rangle$ increase slightly at first and then decrease quickly with the increase in n_{cp}. When a few monomers are adsorbed on the NP, the adsorbed polymers are stretched, resulting in the initial small increase in $\langle R_G^2\rangle$. The adsorption usually takes place at the end monomers of polymer because such a configuration has larger configuration entropy S than that adsorbed at the middle monomers. A

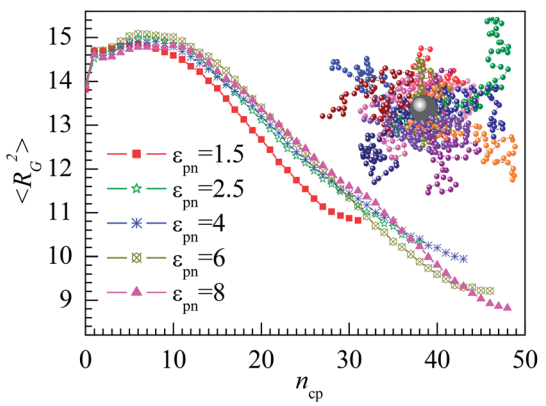

Fig. 2 Dependence of mean square radius of gyration $\langle R_G^2\rangle$ of adsorbed polymers on the number of polymer–NP contacts n_{cp}. The inset presents the snapshot of several adsorbed polymers around the NP for $\varepsilon_{pn} = 3$. NP mobility $\mu = 0$.

snapshot of adsorbed polymers at $\varepsilon_{pn} = 3$ is presented in the inset of Fig. 2. When more and more monomers are adsorbed on the NP, the size of polymers will become smaller and smaller. These observations are in general agreement with our previous simulation results.[43]

3.2. Distribution of monomers

The adsorption of polymers on the NP not only changes the conformation of adsorbed polymers but also changes the number density of monomers around the NP. The number density of monomers ρ is defined as

$$\rho = \frac{n_{r\to r+\Delta r}}{\Delta V_{r\to r+\Delta r}}, \quad (4)$$

where $n_{r\to r+\Delta r}$ is the number of monomers in the region with volume $\Delta V_{r\to r+\Delta r}$ from r to $r + \Delta r$, r is the radial distance from the center of NP and $\Delta r = 0.05\sigma$. Fig. 3A presents the dependence of the relative number density of monomers ρ/ρ_0 on r for several ε_{pn}s. Here ρ_0 is the average density of the system. The distribution of monomers shows four distinct layers denoted as L_1, L_2, L_3, and L_4, respectively. It is clear to see three peaks in the L_1, L_2, and L_3 layers, while ρ/ρ_0 in the L_4 layer keeps a constant. The results indicate that the transition region from the interface to the bulk is between L_3 and L_4 layers. So, in the following text, we define the L_1, L_2, and L_3 layers as the interfacial region. The three interfacial layers have the same width of about 0.8σ, *i.e.*, the interfacial thickness is about 2.4σ.

The distribution of monomers can be explained by the attraction of NP and the interaction among monomers. The peak in the L_1 layer is mainly attributed to the attraction of NP as the NP–monomer distance is very short in this region. Thus, the influence of NP on the L_1 layer is the most important, and the peak of the L_1 layer increases significantly with ε_{pn}. Although the adsorbed monomers will pull the polymer near the NP because of the FENE interaction, the excluded volume effect of polymers pushes them away, which results in the peaks in the L_2 and L_3 layers. The two peaks are however microscopic because of large volumes of the L_2 and L_3 layers relative to that of the L_1 layer. Also, the two peaks are independent of ε_{pn} because of the weak attraction of NP at the relative long NP–monomer distance. The monomers near the NP are adsorbed compactly on the NP, whereas those far away from the NP are loosely distributed, as shown in the inset of Fig. 2. For the monomers in the L_4 layer, the NP–monomer distance is larger than the cut-off distance r_c, and the influence of NP on monomers can be neglected. Also, at the junction of L_1 and L_2 layers, ρ/ρ_0 exhibits a valley due to the repulsion of monomers in the L_1 layer. As the number of monomers in the L_1 layer increases with ε_{pn}, the valley becomes deeper.

The influence of NP size and chain length on the distribution of monomers is also studied. For chain length $n = 64$, we calculated the distribution of interfacial monomers for different NP sizes. Fig. 4A–C present the dependence of the relative number density of monomers ρ/ρ_0 on r for $\sigma_n = 1$, 4, and 6, respectively. For NP size $\sigma_n = 5$, we calculated the distribution of interfacial monomers for different chain lengths. Fig. 4D presents the dependence of ρ/ρ_0 on r for $n = 8$, 48, and 80, respectively. We can see that the interfacial area also can be divided into three layers and the layer width is about 0.8σ. That is to say, the distribution of monomers around NP is independent of the diameter of NP and the chain length of the polymer, which is different from the experiment results. Dielectric spectroscopy found that the interfacial layer thickness increases with the diameter of NP.[33,34] We conjecture that the different results between simulation and experiment are induced by the difference in concentration of monomers. So we further study the distribution of monomers for $\rho_0 = 0.28$, corresponding to a semi-dilute solution.[35] Fig. 3B shows the dependence of ρ/ρ_0 on the radial distance r from the NP center. We can also see three interfacial layers where ρ/ρ_0 is uneven. Compared with the

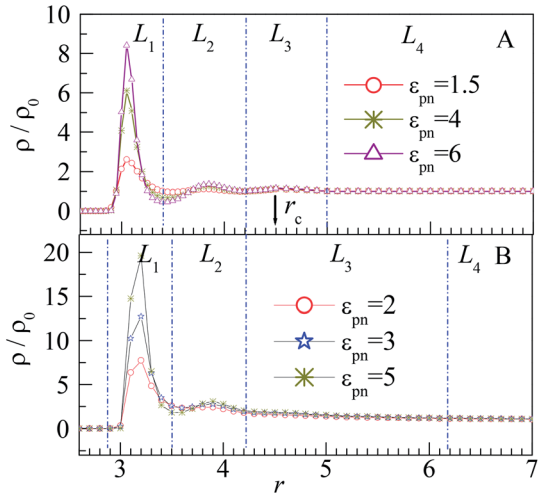

Fig. 3 Relative number density of monomers ρ/ρ_0 *vs.* radial distance r from the center of NP for different ε_{pn}s at (A) $\rho_0 = 0.85$ and (B) $\rho_0 = 0.28$. The blue dash dotted lines separate the system into four layers. The arrow indicates the place of $r_c = 4.5\sigma$. NP mobility $\mu = 0$.

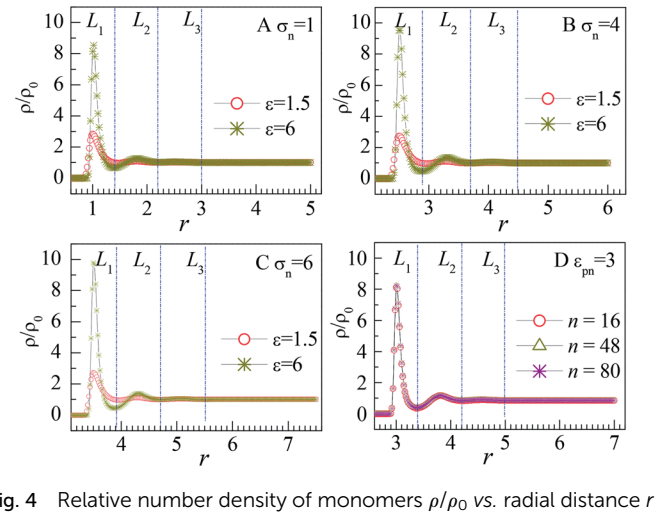

Fig. 4 Relative number density of monomers ρ/ρ_0 *vs.* radial distance r from the center of NP for (A) different ε_{pn}s at $\sigma_n = 1$ and $n = 64$, (B) different ε_{pn}s at $\sigma_n = 4$ and $n = 64$, (C) different ε_{pn}s at $\sigma_n = 6$ and $n = 64$, and (D) different chain lengths n at $\varepsilon_{pn} = 3$ and $\sigma_n = 5$. NP mobility $\mu = 0$.

interfacial layers at $\rho_0 = 0.85$, the three interfacial layers have different thickness. Interestingly, the L_3 layer has a very wide range with $\rho/\rho_0 > 1$, resulting in a larger size interfacial region. That is to say, the concentration of polymer plays an important role on the interfacial layer thickness, which is consistent with the experimental findings.[33] The difference in interfacial layer thickness can be explained from the competition between the chain crowding and the NP size. The chain crowding imposes stronger steric hindrances at the NP surfaces and reduces the interfacial layer thickness, whereas the larger NP has the larger volume-to-surface ratio and can increase the interfacial layer thickness. At $\rho_0 = 0.85$, the chain crowding dominates and the effect of NP size can be neglected. Therefore, we only present our simulation results for $\sigma_n = 5\sigma$ and $n = 64$ in this paper.

3.3. Mobility of interfacial monomers

To gain insight into the mobility of interfacial monomers, we calculate the mean square displacement (MSD) of monomers, which is defined as

$$\langle \Delta r^2 \rangle = \langle [r\rightarrow(t) - r\rightarrow(0)]^2 \rangle, \quad (5)$$

where $r\rightarrow(t)$ and $r\rightarrow(0)$ are the position vectors of monomer at time t and $t = 0$, respectively. Every monomer owns its owner time. We monitor the positions of all monomers. And $t = 0$ is set when the monomer moves into a specific interfacial layer. Then we calculate the MSD of monomers in the three interfacial layers separately. Fig. 5A–C present the evolutions of MSD of monomers in the three interfacial layers at different ε_{pn}s. We can see that $\langle \Delta r^2 \rangle$ increases with the residence time t. The monomers can keep a normal diffusion in all the three interfacial layers. All the residence time scales are very short, and the maximal $\langle \Delta r^2 \rangle$ is very small. The reason is that monomers leave their initial layer easily due to the small thickness of the interfacial layers. The residence time scale and maximal $\langle \Delta r^2 \rangle$ in the L_1 layer are maximum, whereas those in the L_3 layer are minimum. Moreover, the influence of polymer–NP interaction on the diffusion of monomers is investigated. The MSD decreases remarkably with the increase in ε_{pn} in the L_1 layer as shown in Fig. 5A, whereas it is independent of ε_{pn} in the L_3 layer as shown in Fig. 5C. The results indicate that the polymer–NP interaction plays an important role on the diffusion of monomers located close to the NP.

The decrease of MSD with increasing ε_{pn} for monomers in the L_1 and L_2 layers indicate that the attraction of NP retards the diffusion of monomers. The number density of monomers ρ in the L_1 layer increases quickly with ε_{pn}, as shown in Fig. 3A. The dynamics of monomers is slowed down by the crowded environment as well as by the strong attractive effect of NP. The attraction of NP can reduce the dynamics of monomers along the radial direction. Thus the mobility in the L_1 layer decreases with an increase in ε_{pn}. The monomers in the L_2 layer may connect with that in the L_1 layer through FENE interaction. Thus the mobility of monomers in the L_2 layer is partly slowed down. But the influence of NP on the monomers dies away for small ε_{pn} or large NP–monomer distance d_{nm}.

It is well known that the monomers in the glass state are immobilized. In comparison with the glass state, the monomers in the interfacial regions can still move even at large ε_{pn}. To investigate the move of monomers in interfacial layers, we count the number of monomers, n_{im}, which are initially in the layer at time $t = 0$. Fig. 6 presents the evolution of the fraction of initial monomers

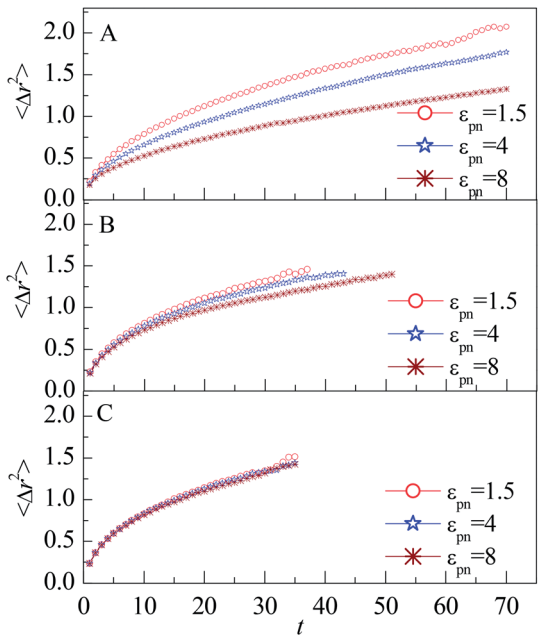

Fig. 5 Mean square displacement of monomers *vs.* the residence time t for monomers in (A) L_1, (B) L_2, and (C) L_3 layers, respectively. NP mobility $\mu = 0$.

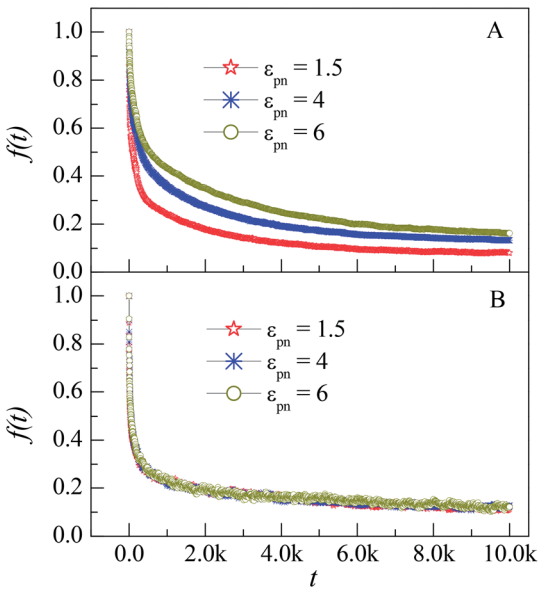

Fig. 6 Dependence of the fraction of initial monomers $f(t)$ on the simulation time t for monomers in the L_1 (A) and L_3 (B) layers at different ε_{pn}s. NP mobility $\mu = 0$.

$$f(t) = \left\langle \frac{n_{\mathrm{im}}(t)}{n_{\mathrm{im}}(0)} \right\rangle \quad (6)$$

in the L_1 and L_3 layers. The properties of $f(t)$ in the L_2 layer are not presented as they are between those in the L_1 layer and in the L_3 layer. We find that $f(t)$ decreases quickly and tends to zero with increasing time t. The results reveal that all the initial monomers in interfacial layers are movable and can jump to other layers even if the attraction is strong. This observer is in general agreement with the experiment results.[24] Also, $f(t)$ is dependent on the polymer–NP interaction strength $\varepsilon_{\mathrm{pn}}$ in the L_1 layer but is roughly independent of $\varepsilon_{\mathrm{pn}}$ in the L_3 layer. It can be understood that as d_{nm} goes up or $\varepsilon_{\mathrm{pn}}$ goes down, the attraction of NP decreases, which leads to the increase in the mobility of monomers.

In our previous works, we have simulated the diffusion of a linear polymer in the sparse environment with periodically distributed NPs.[22] We found that one polymer can be firmly adsorbed on one or two NPs and stop diffusion if the attraction is strong enough. Compared with the monomers in the sparse environment, polymers in the dense environment can always keep in motion. The reason is that only several monomers of a polymer can be adsorbed on the NP because of the crowded environment, as shown in the inset of Fig. 2. The irregular thermal motion of desorption monomers can help the adsorbed monomers to depart from the NP. So there is no glassy state or glassy layer around the NP in the dense environment.

To quantify the effect of polymer–NP interaction on the mobility of monomers, we calculate the half-life period $T_{1/2}$ of $f(t)$ for the three interfacial layers. $T_{1/2}$ means the time duration during which $f(t)$ decreases from 1 to 0.5. Fig. 7 presents the dependence of $T_{1/2}$ on the polymer–NP interaction strength $\varepsilon_{\mathrm{pn}}$. We can see that $T_{1/2}$ increases exponentially with $\varepsilon_{\mathrm{pn}}$ as $T_{1/2} \sim \exp(\alpha\varepsilon_{\mathrm{pn}})$. Here $\alpha = 0.32$, 0.093, and 0.025 for monomers in the L_1, L_2, and L_3 layers, respectively. We know that there is a potential barrier between two neighboring layers. The monomer motion from one layer to another must overcome the potential barrier. The potential barrier height increases with the increase in $\varepsilon_{\mathrm{pn}}$ and the decrease in monomer–NP distance. Thus, the mobility of monomers is sensitive to the attraction of NP in the L_1 layer, and the value of α in the L_1 layer is the largest. In brief, the monomers in the interfacial region exhibit a gradient mobility along the radical direction of NP.

During the dynamical MC simulation, the attempted movements of monomers are accepted according to the Metropolis algorithm. The acceptance probability can also reflect the mobility of monomers. We define the mean probability of monomer movement P_{MM} as

$$P_{\mathrm{MM}} = \left\langle \frac{n_{\mathrm{mm}}}{n_{\mathrm{m}}} \right\rangle. \quad (7)$$

Here n_{m} is the number of monomers in one layer, n_{mm} is the number of monomers accepted to move in the same layer, and $\langle\ \rangle$ represent an ensemble average over all MC steps, respectively. Fig. 8 shows the evolutions of P_{MM} in different layers. In the L_1 layer, P_{MM} is strongly dependent on the polymer–NP interaction strength $\varepsilon_{\mathrm{pn}}$. With the increase in $\varepsilon_{\mathrm{pn}}$, the attraction of NP becomes more potent, and the attempted movement of monomer needs more energy, resulting in an obvious decrease in P_{MM}. However, P_{MM} roughly remains constant in the L_2 and L_3 layers. Moreover, $P_{\mathrm{MM}} \approx 0.64$ in the L_3 layer is roughly the same as that in bulk solution. The results further prove that there is a gradient of monomer mobility in the vicinity of NP.

3.4. Effects of NP mobility

The mobile NP can accelerate the delivery of energy among monomers, which would influence the properties of interfacial polymers and monomers. As NP is heavier than that of monomer, we set $\mu < 1$ in the simulation. We consider several values of NP mobility μ and calculate the interfacial properties for $\varepsilon_{\mathrm{pn}} = 3$. Fig. 9 presents the dependence of the adsorption properties of polymers on the NP mobility μ. $\langle N_{\mathrm{p\_ad}} \rangle$ and $\langle n_{\mathrm{cn}} \rangle$ decrease slowly with an increase in μ, indicating that the adsorption of polymers is weakened by NP mobility. The decrease in $\langle D_{\mathrm{ap}} \rangle$ with μ, as shown in the inset of Fig. 9, further proves this point.

However, the NP of $\sigma_{\mathrm{n}} = 5\sigma$ is 125 times as heavy as the monomer if both NP and monomer have the same mass density. The approximate NP mobility is about $\mu = 0.008$ based

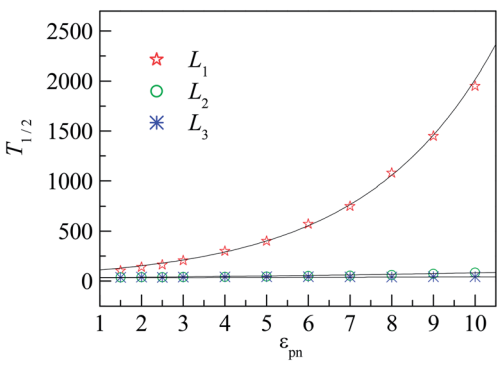

Fig. 7 Dependence of the half-life period $T_{1/2}$ of $f(t)$ on the polymer–NP interaction strength $\varepsilon_{\mathrm{pn}}$ for L_1, L_2, and L_3 layers, respectively. Black curves show the function $T_{1/2} \sim \exp(\alpha\varepsilon_{\mathrm{pn}})$ for monomers in the L_1, L_2, and L_3 layers, respectively. NP mobility $\mu = 0$.

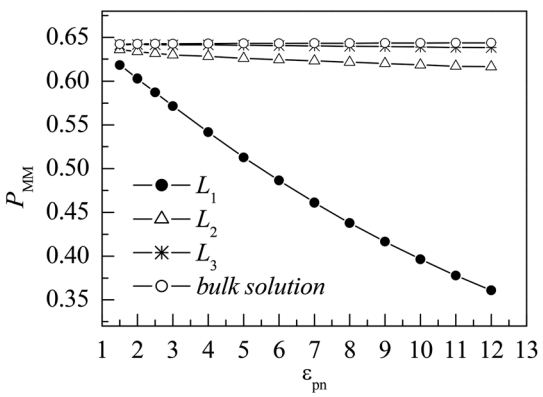

Fig. 8 Dependence of the mean probability of monomer movement P_{MM} on the polymer–NP interaction strength $\varepsilon_{\mathrm{pn}}$ for monomers in the three interfacial layers and the bulk solution. NP mobility $\mu = 0$.

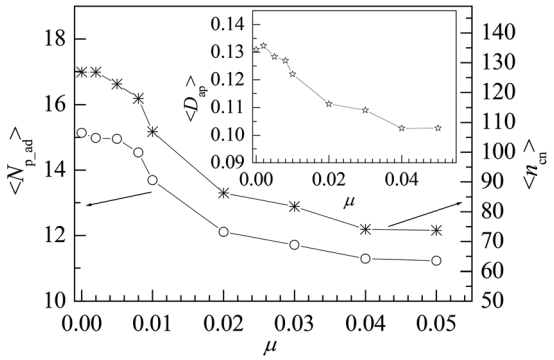

Fig. 9 Dependence of the mean number of adsorbed polymers $\langle N_{p\_ad} \rangle$ and the mean number of total adsorbed monomers $\langle n_{cn} \rangle$ on the NP mobility μ. The inset presents the dependence of the mean adsorption degree of adsorbed polymers $\langle D_{ap} \rangle$ on μ. Here $\varepsilon_{pn} = 3$.

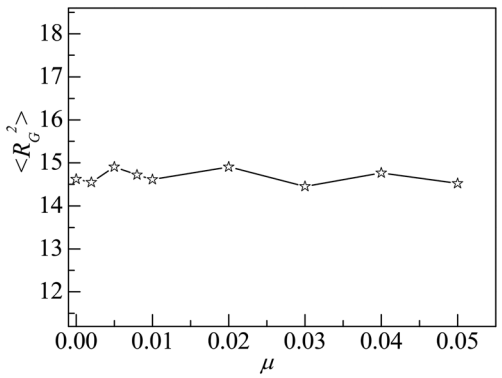

Fig. 10 Mean square radius of gyration $\langle R_G^2 \rangle$ of adsorbed polymers *vs.* the NP mobility μ. Here $\varepsilon_{pn} = 3$.

on the conservation of momentum. From Fig. 9, we can see that there is no remarkable difference in adsorption properties between the polymers at $\mu = 0.008$ and $\mu = 0$. Also, we study the distribution of interfacial monomers for different NP mobility μ at $\varepsilon_{pn} = 3$. The results show that the relative number density of monomers ρ/ρ_0 has the same behaviors as that at $\mu = 0$ shown in Fig. 3A. The conformational properties of adsorbed polymers are also calculated for different NP mobility μ at $\varepsilon_{pn} = 3$. Fig. 10 presents the dependence of $\langle R_G^2 \rangle$ on μ. $\langle R_G^2 \rangle$ keeps nearly a constant, indicating that the tiny change of $\langle D_{ap} \rangle$ caused by the NP mobility has no apparent effect on the conformation of adsorbed polymers and the distribution of interfacial monomers. The dependence of the mobility of interfacial monomers on the NP mobility μ will be investigated in the future.

4. Conclusions

In this work, the conformational and dynamic properties of polymers around the NP are studied using dynamic MC simulations. The polymer–NP interaction ε_{pn} is taken into account as the main factor. Simulations are carried out at high ε_{pn} above the critical adsorption point $\varepsilon_{pn}^* = 1.5$. The adsorption and the conformation of polymers are dependent on the polymer–NP interaction strength ε_{pn}. With an increase in ε_{pn}, the mean number of adsorbed polymers $\langle N_{p\_ad} \rangle$ decreases, whereas the mean number of total adsorbed monomers $\langle n_{cn} \rangle$ and the mean adsorption degree $\langle D_{ap} \rangle$ of adsorbed polymers increase. The results indicate that the increased adsorbed monomers can push away some initially adsorbed polymers. The mean square radius of gyration $\langle R_G^2 \rangle$ of adsorbed polymers decreases with increasing ε_{pn}, indicating that the NP can shrink the conformational size of adsorbed polymers.

By analyzing the number density of monomers ρ along the radial direction of NP, we find that the interfacial region can be divided into three layers marked as L_1, L_2, and L_3, respectively. The interfacial layer thickness is independent of the NP size and the chain length because of the chain crowding. By analyzing the mean square displacement (MSD), the fraction of initial monomers $f(t)$, and the mean probability of monomer movement P_{MM}, we find that the mobility of monomers increases with the decrease in ε_{pn}. Also, we find that the monomers in interfacial layers always keep moving, and there is no glassy layer around the NP. Finally, we have checked the influence of the mobility of NP on the interfacial properties of polymer chains. Results show that the motion of NP can weaken the adsorption of polymers but does not change the conformational property of adsorbed polymers.

Conflicts of interest

The authors declare that they have no conflicts of interest.

Acknowledgements

This work was supported by the National Natural Science Foundation of China under Grant No. 11674277 and 11974305. Computer simulations were carried out in the High Performance Computing Center of Hangzhou Normal University, College of Science and High Performance Computing Center of Lishui University.

References

1 E. M. Zirdehi, T. Voigtmann and F. Varnik, *J. Phys.: Condens. Matter*, 2020, **32**, 275104.
2 N. Suzuki, M. B. Zakaria, Y. D. Chiang, K. C. W. Wu and Y. Yamauchi, *Phys. Chem. Chem. Phys.*, 2012, **14**, 7427–7432.
3 M. K. Crawford, R. J. Smalley, G. Cohen, B. Hogan, B. Wood, S. K. Kumar, Y. B. Melnichenko, L. He, W. Guise and B. Hammouda, *Phys. Rev. Lett.*, 2013, **110**, 196001.
4 J. P. Jose and S. Thomas, *Phys. Chem. Chem. Phys.*, 2014, **16**, 20190–20201.
5 N. Begam, D. A. Nimmi, S. Chandran, M. Ibrahim, V. Padmanabhan, M. Sprung and J. K. Basu, *Soft Matter*, 2018, **14**, 8853–8859.
6 Q. He, Y. J. Zhou, G. F. Wang, B. Zheng, M. Qi, X. J. Li and L. H. Kong, *Appl. Nanosci.*, 2018, **8**, 2009–2020.
7 P. Pornprasit, W. Pechurai, N. Chiangraeng, C. Randorn, N. Chandet, P. Mungkornasawakul and P. Nimmanpipug, *Chiang Mai J. Sci.*, 2018, **45**, 2195–2200.

8 F. W. Starr, T. B. Schroder and S. C. Glotzer, *Phys. Rev. E*, 2001, **64**, 021802.
9 F. Varnik and T. Franosch, *J. Phys.: Condens. Matter*, 2016, **28**, 133001.
10 A. Papon, H. Montes, M. Hanafi, F. Lequeux, L. Guy and K. Saalwachter, *Phys. Rev. Lett.*, 2012, **108**, 065702.
11 P. P. Pandey, *Soft Nanosci. Lett.*, 2015, **5**, 3–11.
12 W. D. Tian and Y. Q. Ma, *Chem. Soc. Rev.*, 2014, **42**, 705–727.
13 L. S. Mbathan and M. Singh, *J. Nanosci. Nanotechnol.*, 2019, **19**, 1959–1970.
14 J. Y. Zhu, G. Wang, C. S. Alves, H. Tomas, Z. J. Long, M. W. Shen, J. Rodrigues and X. Y. Shi, *Langmuir*, 2018, **34**, 12428–12435.
15 K. S. Soppimath, T. M. Aminabhavi, A. R. Kulkarni and W. E. Rudzinski, *J. Controlled Release*, 2001, **70**, 1–20.
16 S. K. Lai, D. E. O'Hanlon, S. Harrold, S. T. Man, Y. Y. Wang, R. Cone and J. Hanes, *Proc. Natl. Acad. Sci. U. S. A.*, 2007, **104**, 1482–1487.
17 V. Sorichetti, V. Hugouvieux and W. Kob, *Macromolecules*, 2018, **51**, 5375–5391.
18 I. Brigger, C. Dubernet and P. Couvreur, *Adv. Drug Delivery Rev.*, 2008, **54**, 631–651.
19 K. Cho, X. U. Wang, S. Nie and D. M. Shin, *Clin. Cancer Res.*, 2008, **14**, 1310–1316.
20 A. I. Nakatani, W. Chen, R. G. Schmidt, G. V. Gordon and C. C. Han, *Polymer*, 2001, **42**, 3713–3722.
21 A. Tuteja, P. M. Duxbury and M. E. Mackay, *Phys. Rev. Lett.*, 2008, **100**, 077801.
22 C. Y. Li, C. J. Qian, Q. H. Yang and M. B. Luo, *J. Chem. Phys.*, 2014, **140**, 104902.
23 C. Y. Li, M. B. Luo, J. H. Huang and H. Li, *Phys. Chem. Chem. Phys.*, 2015, **17**, 31877–31886.
24 A. P. Holt, J. R. Sangoro and A. P. Sokolov, *Macromolecules*, 2015, **47**, 1837–1843.
25 S. Mohammadreza, P. Mehdi, S. K. Mehdi and A. Abbas, *Iran. Polym. J.*, 2013, **22**, 155–163.
26 T. F. Hao, Z. P. Zhou, Y. Wang, Y. Liu, D. Zhang, Y. J. Nie, Y. Wei and S. J. Li, *Monatsh. Chem.*, 2017, **148**, 1285–1293.
27 M. Vacatello, *Macromolecules*, 2001, **34**, 1946–1952.
28 M. Vacatello, *Macromolecules*, 2002, **35**, 8191–8193.
29 J. H. Huang, Z. F. Mao and C. J. Qian, *Polymer*, 2006, **47**, 2928–2932.
30 X. W. Huang, Y. Peng, J. H. Huang and M. B. Luo, *Phys. Chem. Chem. Phys.*, 2017, **19**, 29975–29983.
31 Y. Peng, H. Zhang, X. W. Huang, J. H. Huang and M. B. Luo, *Phys. Chem. Chem. Phys.*, 2018, **20**, 26333–26343.
32 W. P. Cao, L. Z. Sun, C. Wang and M. B. Luo, *J. Chem. Phys.*, 2011, **135**, 174901.
33 A. P. Holt, V. Bocharova, S. Cheng, A. M. Kisliuk, B. T. White, T. Saito, D. Uhrig, J. P. Mahalik, R. Kumar, A. E. Imel, T. Etampawala, H. Martin, N. Sikes, B. G. Sumpter, M. D. Dadmun and A. P. Sokolov, *ACS Nano*, 2016, **10**, 6843–6852.
34 S. Gong, Q. Chen, J. F. Moll, S. K. Kumar and R. H. Colby, *ACS Macro Lett.*, 2014, **3**, 773–777.
35 G. Allegra, G. Raos and M. Vacatello, *Prog. Polym. Sci.*, 2008, **33**, 683–731.
36 Q. Zhang and L. Archer, *Macromolecules*, 2004, **37**, 1928–1936.
37 Q. Zhang and L. Archer, *Langmuir*, 2002, **18**, 10435–10442.
38 Z. Zhu, T. Thompson, S. Q. Wang, E. D. von Meerwall and A. Halasa, *Macromolecules*, 2005, **38**, 8816–8824.
39 K. Kremer and G. S. Grest, *J. Chem. Phys.*, 1990, **92**, 5057–5086.
40 D. Gersappe, *Phys. Rev. Lett.*, 2002, **89**, 058301.
41 V. Guerra and D. Marinov, *Plasma Sources Sci. Technol.*, 2016, **25**, 045001.
42 C. Y. Li, W. P. Cao, M. B. Luo and H. Li, *Colloid Polym. Sci.*, 2016, **294**, 1001–1009.
43 C. Y. Li, M. B. Luo, H. Li and W. P. Cao, *Colloid Polym. Sci.*, 2017, **295**, 2251–2260.

